Front. Phys. 13(5), 138206 (2018)
https://doi.org/10.1007/s11467-018-0776-0

RESEARCH ARTICLE

Reconceptualizing kinesin's working cycle as separate chemical and mechanical processes

Hui-Juan Xu[1,2], Tong Tong[1,2], Rui-Zheng Hou[1,2,†], Hong-Rong Li[1,2]

[1] *School of Science, Xi'an Jiaotong University, Xi'an 710049, China*
[2] *Institute of Quantum Optics and Quantum Information, Xi'an Jiaotong University, Xi'an 710049, China*
Corresponding author. E-mail: †houruizheng@xjtu.edu.cn
Received November 30, 2017; accepted March 7, 2018

The biomolecular motor kinesin uses chemical energy released from a fuel reaction to generate directional movement and produce mechanical work. The underlying physical mechanism is not fully understood yet. To analyze the energetics of the motor, we reconceptualize its chemomechanical cycle in terms of separate fuel reaction and work production processes and introduce a thermodynamic constraint to optimize the cycle. The model predicts that the load dependences of the motor's velocity, stepping ratio, and dwell time are determined by the mechanical parameters of the motor–track system rather than the fuel reaction rate. This behavior is verified using reported experimental data from wild-type and elongated kinesins. The fuel reaction and work production processes indicate that kinesin is driven by switching between two chemical states, probably following a general pattern for molecular motors. The comparison with experimental data indicates that the fuel reaction processes are close to adiabatic, which is important for efficient operation of the motor. The model also suggests that a soft, short neck linker is important for the motor to maintain its load transport velocity.

Keywords kinesin, chemomechanical coupling, thermodynamics, entropy production

PACS numbers 82.39.Fk, 87.16.Nn

1 Introduction

Kinesin is a motor protein that moves along a polymeric track for intracellular transport [1, 2]. It comprises a pair of identical global domains (heads) connected by two flexible peptide chains (neck linkers) [3, 4]. Using this structure, kinesin makes successive steps in hand-over-hand fashion toward the plus end of the track (microtubule). The two heads contact with the track and catalyze fuel (adenosine triphosphate, ATP) by the hydrolysis reaction to obtain energy. The motion of kinesin along the track is rapid and highly directional; it has a speed of ∼100 step/s [5–8], and the probability of making a backward step is only ∼1/1000 [6–8]. In transport, kinesin can support a load of up to ∼7 pN with an energy efficiency of ∼70% [5–8]. The excellent performance has attracted much research interest in the motor's internal working mechanism [9–16].

During a forward step, kinesin undergoes a tightly coupled chemomechanical cycle composed of multistep catalysis in the fuel reaction and a series of conformational changes that generate displacement and work [9–11, 17, 18]. Interaction of the chemical and mechanical processes is a key to the working mechanism. Catalysis of the fuel reaction and the accompanying conformational changes have been studied extensively using experiments [5–7, 18–21] and theoretical models [9–16]. The chemomechanical coupling is often interpreted as simultaneous occurrence of a catalysis step and the induced conformational change. However, recent studies provide some evidence that the coupled chemical and mechanical processes occur successively. First, it was theoretically proposed [22] that the optimized cycle of kinesin is connected by two adiabatic processes, in which the entropy of the system does not increase, and two mechanical processes, in which displacement and work are generated. The behavior predicted by the theory is consistent with experimental data, suggesting that the chemomechanical cycle is composed of these two types of processes. Second, an experiment [19] showed that the neck linker zippering that directs forward steps is induced by ATP hydrolysis. This finding changed the previous understanding that zippering depends on ATP binding. Ac-

cording to this new observation, the chemomechanical cycle is composed of ATP binding and hydrolysis followed by neck linker zippering, as well as release of the hydrolysis products [adenosine diphosphate (ADP) and inorganic phosphate (Pi)] followed by rear head detachment from the track. This order forms a "drive–move" pattern. Therefore, the two types of processes in the theory are likely to be specific to the fuel reaction and work production. On the basis of the above analysis, a cycle with these chemical and mechanical processes can be formulated, which may simplify theoretical analysis of the chemomechanical cycle and provide thermodynamic information for understanding the underlying physical mechanism.

In this paper, we reconceptualize the chemomechanical cycle of kinesin in terms of separate fuel reaction and work production processes. The model is formulated using the kinetics. The dependence of the kinetic rates on the input chemical energy and output mechanical work are given by the detailed balance condition. Entropy production as defined by the kinetics [23, 24] is used to quantify the energy dissipation in the processes, and a thermodynamic constraint [22] on the entropy production is introduced to optimize the directional fidelity of the motor. With the reconceptualized cycle and the thermodynamic constraint, the expressions for the motor's velocity, stepping ratio, and dwell time show a common feature; namely, their load dependences rely mainly on the mechanical parameters of the motor–track system and are not influenced by the fuel reaction rates. The predicted feature is tested by a comparison with reported experimental data from wild-type and elongated kinesins, which supports the reconceptualized cycle. The reconceptualized cycle indicates that kinesin is driven by switching between two chemical states, probably following a general pattern for molecular motors. When the model results are fitted to the experimental data, the model yields low entropy production in the fuel reaction processes, which suggests that these processes are close to adiabatic. The model also suggests that the soft, short neck linkers play an important role in maintaining the load transport velocity of kinesin.

2 Kinetic model

2.1 Reconceptualized chemomechanical cycle

The cycle (Fig. 1) starts with an ATP-waiting state, where one head waits for ATP binding and is strongly attached to the track, and the other head binds with ADP and diffuses to search for the next association site on the track. ATP binding and subsequent hydrolysis ($1 \rightarrow 2$) induce zippering of the neck linker, which directs the diffusing head to attach to the forward site on the track ($2 \rightarrow 3$). After attaching, the head takes the leading position, which causes it to release ADP and become strongly attached to the track. The other head, which falls to the rear position, releases the hydrolysis product Pi ($3 \rightarrow 4$); consequently, the head contains the remaining ADP and becomes weakly attached to the track. Hence, ADP and Pi release switch the head-track attachment strength between the front and rear heads, and induce the rear head to detach from the track ($4 \rightarrow 1$). Finally, the motor returns to the initial state but hydrolyzes one ATP molecule and takes one step forward along the track. If a load is attached to the motor, mechanical work is performed in the forward step. The order of the processes in the cycle is adopted from an experiment [19], and the corresponding fuel reaction ($1 \rightarrow 2$ and $3 \rightarrow 4$) and work production ($2 \rightarrow 3$ and $4 \rightarrow 1$) processes are described by our reconceptualization.

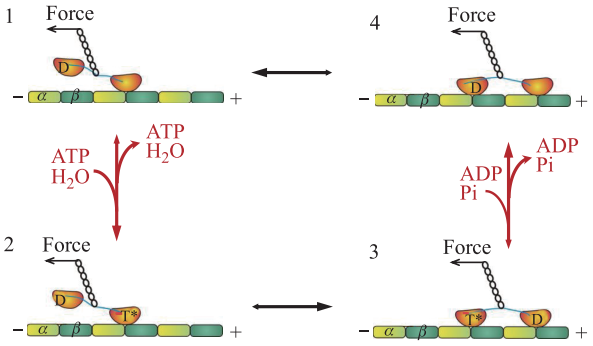

Fig. 1 Illustration of the reconceptualized chemomechanical cycle for kinesin. The shown biped is kinesin. The plump foot is the motor head. The blue line connecting the two plump feet is the necklinker. The short red line (in state 2 & 3) on the necklinker denotes the zippering effect. The helical structure in the middle of the necklinker is the coiled coil which dimerizes the two motor heads. Load force (f) is attached through the coiled coil to the middle of the neck linker. The track is the microtubule filament. The symbols T and D on the motor head denote ATP and ADP respectively. The symbols α and β on the track denote the subunits of α-tubulin and β-tubulin which compose the microtubule filament. The symbols of '+' and '−' denote the forward and the backward directions of the track. The red arrows associated with ATP, ADP, Pi and H_2O denote the fuel reactions, which is catalyzed by the motor head. The black arrows denote the mechanical processes of head detaching from track as well as head binding to track, which are coupled with the load force.

2.2 Kinetics and thermodynamics of the model

A transition from one state (i) to another (j) is assigned a transition rate (k_{ij}). All transitions are assumed to be

reversible ($k_{ij} \leftrightarrow k_{ji}$). According to the reconceptualization of the cycle, the transition rates for the fuel reaction processes ($1 \to 2$ and $3 \to 4$) depend on the chemical energy ($\Delta\mu'$) provided by the fuel, and the transition rates for the work production processes ($2 \to 3$ and $4 \to 1$) depend on the mechanical work produced by the motor (fd). The relations are generated using the detailed balance condition as follows:

$$\Delta F_{12} + \Delta F_{34} + \Delta\mu' = k_B T \ln \frac{k_{12}k_{34}}{k_{21}k_{43}}, \tag{1}$$

$$\Delta F_{23} + \Delta F_{41} - fd = k_B T \ln \frac{k_{23}k_{41}}{k_{32}k_{14}}. \tag{2}$$

ΔF_{ij} is the difference in the free energy of the motor between state i and state j; f is the load force, d is the step size (~8 nm), k_B is the Boltzmann constant, and T is the environmental temperature (~300 K). After one cycle, the total free-energy change of the motor equals zero: $\Delta F_{12} + \Delta F_{23} + \Delta F_{34} + \Delta F_{41} = 0$. Both ΔF_{23} and $-\Delta F_{41}$ are composed of the head-track binding energy for the ADP-bound head and the free energy of the extended neck linker (Fig. 1). The free energy of neck linker zippering is ignored because it is very small ($\sim 1k_BT$) [4]. Hence, $\Delta F_{23} + \Delta F_{41} = 0$, and $\Delta F_{12} + \Delta F_{34} = 0$, so Eqs. (1) and (2) can be simplified as follows:

$$\Delta\mu' = k_B T \ln \frac{k_{12}k_{34}}{k_{21}k_{43}}, \tag{3}$$

$$-fd = k_B T \ln \frac{k_{23}k_{41}}{k_{32}k_{14}}. \tag{4}$$

After a cycle, a portion of the chemical energy from the fuel is used to do work, and the rest is dissipated. The dissipated energy is quantified in terms of the entropy production as follows:

$$\Delta\mu' - fd = T(\Delta S_{12} + \Delta S_{23} + \Delta S_{34} + \Delta S_{41}). \tag{5}$$

ΔS_{ij} is the entropy production of a transition from state i to state j, which is defined as $\Delta S_{ij} = k_B \ln(p_i k_{ij}/p_j k_{ji})$ [23, 24], and p_i is the probability that the motor is in state i. According to the definition of the entropy production, ΔS_{23} and ΔS_{41} quantify the stepping bias of the motor, so the two entropy production values determine the directional fidelity of the motor. Because the sum of the two entropy production values is always limited, namely, $T(\Delta S_{23} + \Delta S_{41}) < \Delta\mu' - fd$ (Eq. 5), optimizing the motor's directional fidelity requires $\Delta S_{23} = \Delta S_{41}$ [22]. In this model, the condition for optimization is introduced. The entropy production values of the two fuel reaction processes are also assumed to be equal, that is, $\Delta S_{12} = \Delta S_{34}$. The sum $\Delta S_{\mathrm{C}}^0 = \Delta S_{12}^0 + \Delta S_{34}^0$ is treated as a fitting parameter, where 0 indicates that no load is attached.

2.3 Assignment of kinetic rates

The transition rates are assigned to satisfy Eqs. (3) and (4) and the two conditions for entropy production. The ATP, ADP, and Pi binding rates are proportional to their concentrations, that is, $k_{12} = k_{\mathrm{ATPb}}[\mathrm{ATP}]$ and $k_{43} = (1/k_{\mathrm{ADPb}}[\mathrm{ADP}] + 1/k_{\mathrm{Pib}}[\mathrm{Pi}])^{-1}$. The square brackets denote the concentrations, and k_{ATPb}, k_{ADPb}, and k_{Pib} are the binding coefficients. The reversed rates, k_{21} and k_{34}, are constants that satisfy Eq. (3). The transition rates of the work production processes depend on the attached load according to a Boltzmann relationship, namely, $k_{ij} = k_{ij}^0 e^{-f\delta_{ij}/k_BT}$, where k_{ij}^0 is the rate without a load attached, and δ_{ij} is the load-coupling distance. The load-coupling distances satisfy $\delta_{23} - \delta_{32} + \delta_{41} - \delta_{14} = d$ according to Eq. (4). The load-coupling distances are also constrained by the two conditions for entropy production according to the relations below (Methods):

$$\frac{k_{14}}{k_{12}} = \frac{1 - \mathrm{e}^{-\Delta S_{12}/k_B}}{\mathrm{e}^{\Delta S_{41}/k_B} - 1}, \quad \frac{k_{23}}{k_{21}} = \frac{\mathrm{e}^{\Delta S_{12}/k_B} - 1}{1 - \mathrm{e}^{-\Delta S_{23}/k_B}},$$
$$\frac{k_{32}}{k_{34}} = \frac{1 - \mathrm{e}^{-\Delta S_{34}/k_B}}{\mathrm{e}^{\Delta S_{23}/k_B} - 1}, \quad \frac{k_{41}}{k_{43}} = \frac{\mathrm{e}^{\Delta S_{34}/k_B} - 1}{1 - \mathrm{e}^{-\Delta S_{41}/k_B}}. \tag{6}$$

All four entropy productions are load-dependent. Eq. (6), in combination with the relations $\Delta S_{23} = \Delta S_{41}$ and $\Delta S_{12} = \Delta S_{34}$, requires the same load dependence for k_{23} and k_{41} and the same load dependence for k_{32} and k_{14}. Hence, $\delta_{23} = \delta_{41}$, $\delta_{32} = \delta_{14}$, and $\delta_{23} - \delta_{32} = \delta_{41} - \delta_{14} = d/2$. δ_{23} is treated as the independent parameter, and the load dependence of $\delta_{23} = \delta_0 + \varepsilon f$, where δ_0 is the distance for zero load, and ε is the elongation coefficient of the distance for the attached load. The worm-like chain model [25] gives $\varepsilon = l_p l_c/(2k_BT)$ (Methods), where l_p and l_c are the persistence length and contour length of the neck linker, respectively.

3 Results and discussion

3.1 Expressions for kinesin's behavior according to the model

On the basis of the kinetic model, analytical expressions for kinesin's velocity, forward versus backward stepping ratio, and dwell time are derived. Assuming that the energy dissipation ($T\Delta S_{\mathrm{C}}^0$) in the fuel reaction processes is small, the velocity is expressed as (Methods)

$$v = \frac{d[\mathrm{e}^{\Delta S_C^0/(2k_B)} - 1]\mathrm{e}^{-f(\delta_0+\varepsilon f)/(k_BT)}}{\mathrm{e}^{\Delta S_C^0/(2k_B)}(k_{12}^{-1} + k_{34}^{-1}) + k_{21}^{-1} + k_{43}^{-1}}. \tag{7}$$

Eq. (7) contains a prefactor for the dependence of the fuel reaction rates and an exponential factor for the load

dependence. The transition rates for the two mechanical processes do not appear explicitly in the expression. Hence, the fuel reaction rates and load force influence the velocity through the two independent factors. The prefactor is the velocity without a load attached. The functional form of the prefactor indicates that the velocity increases with the fuel concentration through the fuel-binding rate, $k_{12} = k_{\mathrm{ATPb}}[\mathrm{ATP}]$. The load force ($f$) appears only in the exponential factor, so the load dependence of the velocity remains the same for different fuel concentrations. The functional form of the exponential factor suggests a Gaussian-type reduction of the velocity against the load, which relies on the two parameters δ_0 and ε. δ_0 is determined by the configurational change of the neck linker as the diffusing head binds to the track when no load is attached, and ε is determined by the mechanical parameters of the neck linker (l_p and l_c); thus, the load dependence of the velocity is related only to the mechanical parameters of the motor–track system.

The stepping ratio between forward and backward steps is interpreted as the average ratio of all the mechanical transition events in the forward direction versus that of those in the backward direction, namely, $R = (p_2k_{23} + p_4k_{41})/(p_3k_{32} + p_1k_{14})$. The ratio is expressed as (Methods)

$$R = \mathrm{e}^{(\Delta\mu' - T\Delta S_C^0)/(2k_BT)}\mathrm{e}^{-f(d/2)/(k_BT)}. \tag{8}$$

Like Eq. (7), the expression also contains factors for the zero-load stepping ratio and load dependence. The zero-load stepping ratio is determined by the input chemical energy ($\Delta\mu'$) minus the dissipated portion ($T\Delta S_{\mathrm{C}}^0$). The load dependence of the stepping ratio relies only on the characteristic distance of the half-step size ($d/2$), which is determined by the track. This load dependence is different from that of the velocity, in which the elongation coefficient (ε) depends on the parameters of the neck linker. As a consequence of the introduced condition for optimizing the directional fidelity, the derived expression for the stepping ratio is similar to that in Ref. [22].

The average dwell time for a step depends on the motor's velocity and stepping ratio, so the expression for the average dwell time is derived using Eqs. (7) and (8) (Methods):

$$\tau = \frac{\mathrm{e}^{\Delta S_C^0/(2k_B)}(k_{12}^{-1} + k_{34}^{-1}) + k_{21}^{-1} + k_{43}^{-1}}{\mathrm{e}^{\Delta S_C^0/(2k_B)} - 1}\mathrm{e}^{f(\delta_0+\varepsilon f)/(k_BT)}[1 - 2(R+1)^{-1}]. \tag{9}$$

For a small load, the stepping ratio is a large number ($R \gg 1$), so the term $(R+1)^{-1}$ in Eq. (9) can be ignored, and the expression for the average dwell time follows the functional form of the velocity [Eq. (6)] in a reciprocal way. For a large load, the term $(R+1)^{-1}$ can be expanded as $\sum_{n=0}^{\infty}(-R)^n$, and all the terms in the expanded expression contain a factor contributing to the dwell time for zero load and another factor for the load dependence. Hence, in the expressions for the velocity, stepping ratio, and dwell time [Eqs. (7), (8), and (9), respectively), the load dependence of the performance is independent of the fuel reaction rate. This feature is specific to the reconceptualized cycle under the condition of small energy dissipation in the fuel reaction processes.

3.2 Comparison with experimental data

The behavior predicted by the model is compared with reported experimental data [6, 7] from wild-type kinesin, and the key features of the predicted behavior are examined in terms of the comparison. The measured velocity shows approximately the same load dependence for high and low fuel (ATP) concentrations [Figs. 2(a) and (b)]. The measurements also support the predicted Gaussian-type reduction against the load. The velocity predicted by the theory fits the experimental data. The values of the parameters used in the fitting are listed in Table 1. The measured stepping ratio and dwell time also show approximately the same load dependence for high and low fuel (ATP) concentrations. Without adjustment of the parameters, the predicted stepping ratio and dwell time are also consistent with the experimental data [Figs. 2(c)–(f)]. The measured stepping ratio clearly displays a load-coupling distance of ~4 nm, which is just the half-step size of kinesin. This feature is also consistent with the theory [Eq. (7)]. Regarding the dwell time, whereas the theory derives the average dwell time, the measurements give the dwell times for forward and backward steps. However, the difference between the two is small, and their load dependence is similar. The predicted load dependence of the average dwell time fits both measurements well.

In the above comparison, the load-irrelevant parameters are adjusted to fit the experimental data for zero load, and the load-relevant parameters are adjusted to fit the load dependence. The zero-load velocity and dwell time predicted by the model are determined mainly by the fuel-binding coefficient (k_{ATPb}) and the entropy production (ΔS_{C}^0) of the two fuel reaction processes [Eqs. (7) and (9)]. In the fitting, the binding coefficients of the

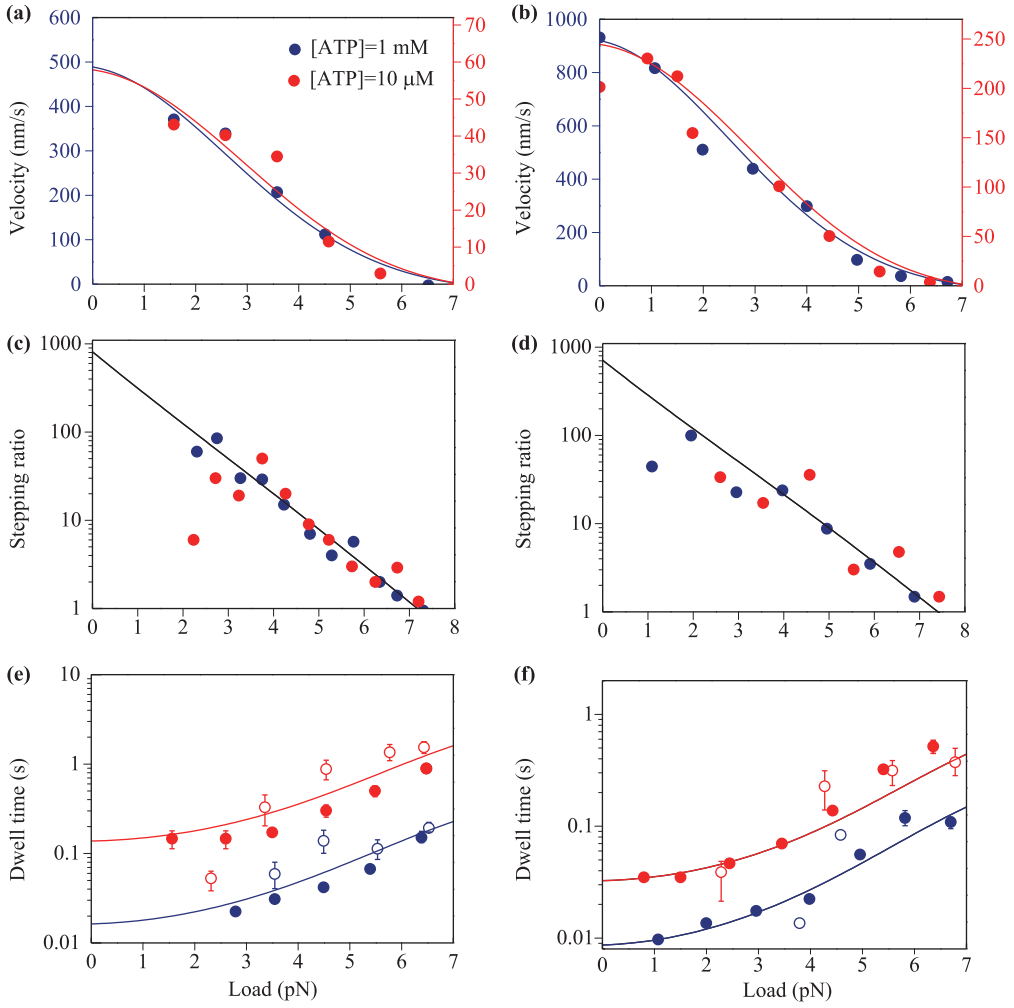

Fig. 2 Predicted performances vs. experimental data. The lines are theoretical predictions and the symbols are experimental data. The blue and the red colors denote the high (1 mM) and the low (10 μM) fuel (ATP) concentrations respectively. **(a, b)** The velocities for the high and the low ATP concentrations refer to the left and the right vertical axes respectively. **(c, d)** The black lines indicate the predicted stepping ratios at the high and low ATP concentrations are overlapped. **(e, f)** The filled and the empty symbols denote the dwell times for forward and backward steps respectively. The experimental data in (a), (c) and (e) are from Ref. [6], and the experimental data in (b), (d) and (f) are from Ref. [7]. $\Delta\mu'$ is taken 14 k_BT for the theoretical predictions.

Table 1 Fitting parameters. WT and EL denote wild-type kinesin and elongated kinesin, respectively. The fittings to the experimental data in Refs. [6, 7] and [17] yield k_{ATPb}, k_{ADPb}, k_{Pib}, k_{21}, $\Delta S_{\mathrm{C}}^{0}$ and l_p. The values of k_{ATPb}, k_{ADPb}, k_{Pib} and k_{21} are close to the measured values in experiment [18]. The value of l_p is close to the measurement in Ref. [26]. The value of l_c is derived by the number of residues (14 for wild-type kinesin and 20 for elongated kinesin) in one necklinker multiplied by the length of one residue (∼0.36 nm).

Expt.	k_{ATPb} (μM/s)	k_{ADPb} (μM/s)	k_{Pib} (μM/s)	k_{21} (1/s)	$\Delta S_{\mathrm{C}}^{0}$ (k_B)	δ_0 (nm)	l_c (nm)	l_p (nm)
[6] WT	4	2.5	1	220	0.65	0.16	5	0.4
[7] WT	14	7	7	220	0.9	0.16	5	0.4
[17] EL	10	7	7	220	0.35	0.16	7.2	0.58

fuel (k_{ATPb}) and the hydrolysis products (k_{ADPb} and k_{Pib}), as well as the fuel release rate (k_{21}), are taken close to the values measured in the experiment [18]. The entropy production $\Delta S_{\mathrm{C}}^{0}$ remains small (∼0.6–0.9 k_B), which is consistent with our assumption of small energy dissipation ($T\Delta S_{\mathrm{C}}^{0}$) in the fuel reaction processes. For small $\Delta S_{\mathrm{C}}^{0}$, the predicted zero-load stepping ratio depends mainly on the input chemical energy $\Delta\mu'$ [Eq. (8)],

which is assigned to fit the experimental data.

The theoretical load dependences of the velocity and dwell time depend on the parameters δ_0, l_c, and l_p. The fitting requires a small value of δ_0, which indicates that the load dependence relies mainly on l_c and l_p. To fit the load dependence, l_c is obtained directly from the number (∼14) of amino acids in one neck linker multiplied by the length (∼0.36 nm) of each amino acid, and the persistence length (l_p) is taken close to the value measured in the experiments [26]. To reproduce the single-exponential load dependence of the stepping ratio, ΔS_C^0 must be a small number, which is again consistent with our assumption regarding $T\Delta S_C^0$. This requirement is discussed in detail in a later section.

To further test the model, we compare its predictions with experimental data from a mutant kinesin with elongated neck linkers and a conserved track [17]. Six amino acids were inserted into each neck linker in the experiment, so l_c is increased, and ε ($= l_p l_c/(2k_BT)$) is enlarged; thus, the theory [Eq. (7)] predicts a faster decrease in the velocity against the load compared to that for the wild-type kinesin. The experimental data for the elongated kinesin indeed display a faster decrease in the velocity against the load [Fig. 3(a)]. Further, the data for the elongated kinesin also show that the load dependence of the velocity is approximately the same at high and low ATP concentrations [Fig. 3(a)]. With the increased l_c (∼ 7.2 nm for 20 amino acids), the predicted velocity fits the experimental data. All the other parameters in the fitting are close to those used for the wild-type kinesin (Table 1). Regarding the stepping ratio, the load dependence relies only on the half-step size according to Eq. (8). Because of the conserved track, the step size of the elongated kinesin remains the same as that of the wild-type kinesin. Therefore, the theory predicts the same load dependence of the stepping ratio for the elongated and wild-type kinesins. Two sets of experimental data ([ATP] = 10 μM and 2 μM) for the elongated kinesin indeed show the same slope as the half-step size [Fig. 3(b)]. Hence, the overall agreement revealed by the comparisons verifies the predicted features of the behavior and supports the reconceptualized cycle for kinesin.

3.3 Energy dissipation in the fuel reaction processes

Our model indicates that the energy dissipation in the fuel reaction processes is small ($T\Delta S_C^0 < 1k_BT$). If large values of the dissipation are used, the theoretical predictions [Eqs. (7), (8), and (9)] deviate from the experimental data. For the stepping ratio in particular, the single-exponential dependence on the load [Eq. (8)] is not valid in the theory for large values of the dissipation. As the dissipation increases, the stepping ratio from the exact solution decreases (Fig. 4), and its load dependence is no longer single-exponential as shown in Eq. (8). In this case, an increased input energy ($\Delta\mu'$) may compensate for the reduction in the stepping ratio [as indicated by Eq. (8)], but it still cannot make the solution fit the experimental data. Hence, the comparison further supports the prediction that the energy dissipation in the fuel reaction processes is small.

The extremely efficient biomolecular motor F_0F_1 (energy efficiency ∼100% [27–29]) also displays a single-exponential load dependence of the stepping ratio [28], and the decreased slope of the dependence is also equal to the half-step size of the motor. Studies [30, 31] that used kinetic models to analyze the motor's chemomechanical cycle also derived small dissipation in the fuel reaction processes. Therefore, advanced biomolecular

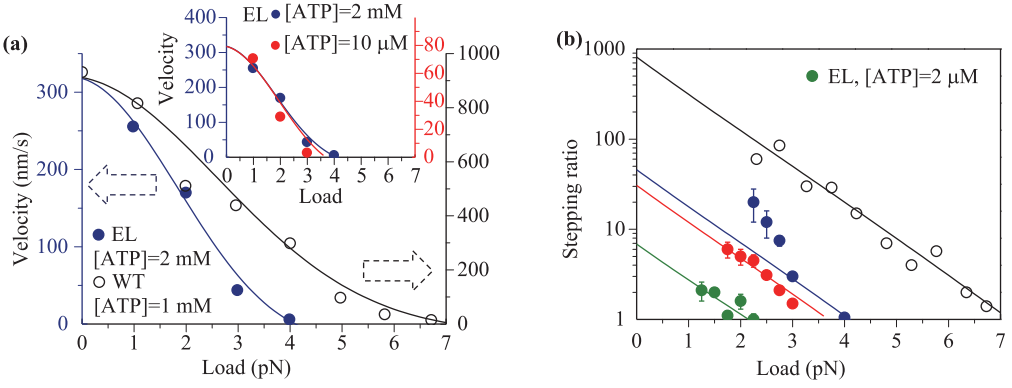

Fig. 3 Performances of elongated kinesin. The lines are theoretical predictions and the symbols are experimental data. **(a)** The large frame shows the comparison between the velocities of the elongated kinesin and the wild-type kinesin. The small frame shows the velocities of the elongated kinesin for the high and the low fuel (ATP) concentrations. **(b)** Comparison between the stepping ratios of the elongated kinesin and the wild-type kinesin. The experimental data of the elongated kinesin are from Ref. [17], and the experimental data of the wild-type kinesin are from Refs. [6, 7]. The predictions for the fuel concentrations of 2 mM, 10 and 2 μM are made by $\Delta\mu'$ of 8, 7 and 4.5 k_BT respectively.

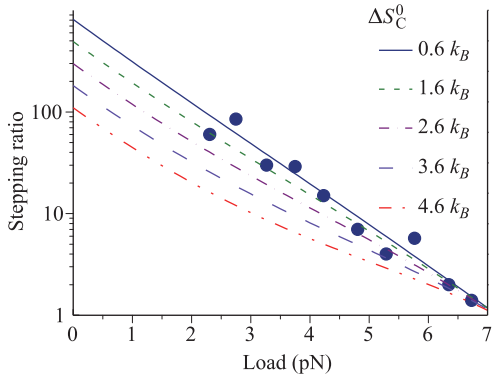

Fig. 4 Analysis of the energy dissipation in the fuel-reaction processes. The lines are predictions from the model with different values of ΔS_C^0. The solid line fits the experimental data using the value of ΔS_C^0 in Table 1, and the dot lines are results from adjusting ΔS_C^0. The symbols are experimental data for high ATP concentration ([ATP] = 1 mM) from Ref. [6].

motors likely dissipate very small amounts of energy during the fuel reaction. In the reconceptualized cycle, the fuel reaction processes do not contribute directly to work production, so the input energy assigned to the processes cannot be used to do work. Hence, the small energy dissipation indicates that most of the input energy is used in the mechanical processes of work production and directional movement, that is, $\Delta\mu' \approx Fd + T(\Delta S_{23} + \Delta S_{41})$, which is ideal for efficient fuel-driven motors.

3.4 Dependence of load transport velocity on the neck linker

An important function of kinesin is intracellular transport. Maintaining high velocity during cargo transport is desirable, so ideally the velocity of kinesin should decrease slowly against the load. Our model suggests that the decrease in the slope depends on the load-coupling distance δ_{23}, which increases with the load force owing to the force-induced extension of the neck linkers. We further test the relation by using a fixed load-coupling distance δ_{23} to fit the measured velocity [Figs. 5(a) and (b)]. The fixed δ_{23} produces an exponential decrease in the load dependence of the velocity, which deviates from the experimental data. In the theory, the load dependence of the dwell time is approximately the reciprocal of that for the velocity [Eqs. (7) and (9)], so the dwell time is also used for the test. The predicted dwell time with the fixed δ_{23} obviously deviates from the experimental data at large loads [Figs. 5(c) and (d)]. These results indicate that the load-coupling distance δ_{23} increases with the load force.

According to the model, the elongation coefficient (ε) depends on the persistence length (l_p) and contour length (l_c) of the neck linker [$\varepsilon = l_p l_c/(2k_BT)$], suggesting that at small values of l_p and l_c, the velocity of kinesin can decrease slowly with increasing load. The neck linker is only a single-peptide chain and thereby is very soft ($l_p < 1$ nm), which satisfies the requirement of a short persistence length. The contour length of the two neck linkers (∼10 nm) must be longer than the step size (∼8 nm), but the ratio of the contour length to the step size is small (∼1.25), which also satisfies the requirement of a short contour length. Hence, the soft, short neck linker supports the ability of kinesin to maintain a relatively high velocity while transporting loads. Regarding the functional roles of the neck linker, studies [12, 32] suggest that its short length is important for kinesin to generate unidirectional motion and output a sufficient amount of work. Therefore, the soft, short neck linker plays an important role in kinesin's transport function.

3.5 Chemomechanical coupling of kinesin

The model provides a picture of two chemical processes and two mechanical processes that interact successively in the chemomechanical cycle. According to our reconceptualization, the fuel inside the two motor heads switches between two chemical states: ADP for one head and no fuel for the other versus ATP for one head and ADP for the other (Fig. 1). The driving mechanism is comparable to that of heat engines, which are driven by switching the temperatures of their working substances that occupy hot and cold reservoirs; that of some artificial molecular motors [33–36], which are driven by switching the frequencies of light to induce molecular isomerization in the motors; and that of the Brownian motor [37], which is driven by switching the external potential between on and off. The similarity indicates that the reconceptualized cycle for kinesin probably follows a general pattern for power machines. Moreover, a recent theory [22] proved that the optimized cycle for kinesin contains two processes with zero entropy production, which are comparable to the two adiabatic processes in the Carnot cycle. This study further suggests that the two processes are specific to the fuel reaction. Hence, the reconceptualized cycle and thermodynamic analysis in this study may provide a new way to see the chemomechanical coupling of kinesin.

The proposed driving mechanism of kinesin can be further tested from other perspectives in the future. To elucidate the working mechanism of kinesin, a recent study [16] developed a rigorous method to analyze multiple cycles that may occur in its operation and showed that there is a single cycle that dominates the working processes. For general kinetic models, the method can derive the probability that each cycle will occur, so it can be used to check the significance of the reconceptualized cycle by general consideration of more possible working cycles. Other biomolecular motors such as myosin V and

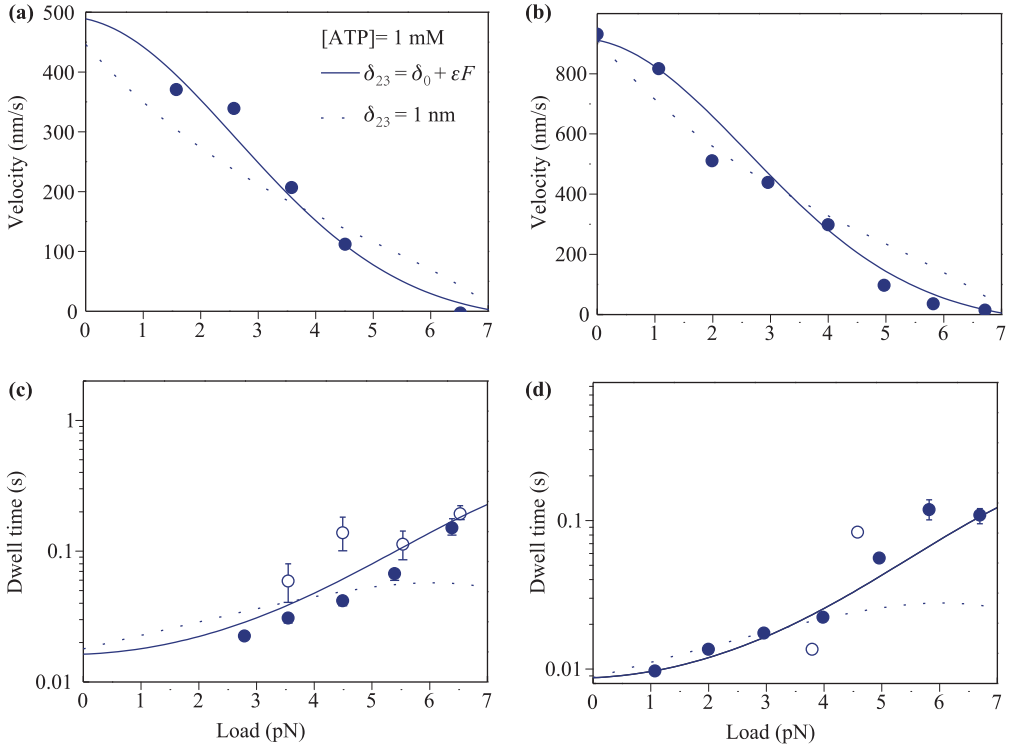

Fig. 5 Analysis of load-coupling distance. The solid lines and dot lines are predictions from the model using respective load-coupling distance $\delta_{23} = \delta_0 + \varepsilon f$ and $\delta_{23} = 1$ nm. Other parameters for the predictions remain the same as in Table 1. The symbols are experimental data from Refs. [6, 7].

F_0F_1 are also driven by the fuel reaction of ATP; their performance data are also abundant [38, 39] and can be used to test the generality of the proposed driving mechanism.

4 Conclusions

In this study, we reconceptualize kinesin's chemomechanical cycle in terms of separate chemical and mechanical processes and introduce a thermodynamic constraint for optimization of the cycle. The model predicts that the load dependences of the motor's parameters are not influenced by the fuel reaction rates but rely only on the mechanical parameters of the motor–track system. The predicted behavior is consistent with reported experimental data from wild-type and mutant kinesins. The reconceptualized cycle suggests that the fuel reaction switches the motor between two chemical states to drive the motion. Thermodynamic analysis indicates that a small amount of energy is dissipated in the fuel reaction processes, and thus most of the input energy can be used to generate motion and work. Therefore, the way that the motor catalyzes the fuel reaction without high dissipation is a key to achieving efficient operation. The information is useful for studies on fuel catalysis in biomolecular motors. The model also quantifies the relation between the load dependence of the velocity and the parameters of the neck linker, and suggests that the soft, short neck linker is important for maintaining the velocity during load transport. This relation might be useful for experimental realization of advanced artificial mimics of the bipedal motor. The overall study may lead to a deeper understanding of the physical mechanism of biomolecular motors.

5 Methods

5.1 Relation between transition rate and entropy production

For a single-pathway cycle, the steady-state condition is $p_i k_{i,i+1} - p_{i+1}k_{i+1,i} = p_{i-1}k_{i-1,i} - p_i k_{i,i-1}$. Further, $p_i k_{ij}$ is the transition flux from state i to state j. By introducing the definition of entropy production, namely, $\Delta S_{ij} = k_B \ln[p_i k_{ij}/(p_j k_{ji})]$, the steady-state condition can be expressed in terms of the transition rates with entropy production:

$$k_{i,i+1}(1 - \mathrm{e}^{-\Delta S_{i,i-1}/k_B}) = k_{i,i-1}(\mathrm{e}^{\Delta S_{i-1,i}/k_B} - 1). \quad (10)$$

Applying Eq. (10) to the four-state model yields Eq. (6).

5.2 Expression for the velocity

The velocity of the motor is equal to the net-transition flux of the cycle multiplied by the step size, $v = d(p_1k_{12} - p_2k_{21})$. The expression is expanded using the steady-state condition ($p_ik_{i,i+1} - p_{i+1}k_{i+1,i} = p_{i-1}k_{i-1,i} - p_ik_{i,i-1}$) and the normalization of the total probability of the four states ($p_1 + p_2 + p_3 + p_4 = 1$):

$$v = d\left(\frac{p_1}{p_1k_{12} - p_2k_{21}} + \frac{p_2}{p_2k_{23} - p_3k_{32}} + \frac{p_3}{p_3k_{34} - p_4k_{43}} + \frac{p_4}{p_4k_{41} - p_1k_{14}}\right)^{-1}. \tag{11}$$

By introducing the definition of entropy production in the four terms on the right-hand side of Eq. (11), as well as the relation in Eq. (6), the velocity is expressed in two equivalent forms:

$$v = d\cdot\left[\frac{k_{21}e^{\Delta S_{12}/k_B} + k_{12}}{k_{12}k_{21}(e^{\Delta S_{12}/k_B} - 1)} + \frac{k_{43}e^{\Delta S_{34}/k_B} + k_{34}}{k_{34}k_{43}(e^{\Delta S_{34}/k_B} - 1)}\right]^{-1}, \tag{12}$$

$$v = d\left[\frac{k_{32}e^{\Delta S_{23}/k_B} + k_{23}}{k_{23}k_{32}(e^{\Delta S_{23}/k_B} - 1)} + \frac{k_{14}e^{\Delta S_{41}/k_B} + k_{41}}{k_{41}k_{14}(e^{\Delta S_{41}/k_B} - 1)}\right]^{-1}. \tag{13}$$

The two equations are exact solutions of the velocity. Eq. (12) is used to derive the velocity at zero load ($f = 0$) for $\Delta S^0_{12} + \Delta S^0_{34} = \Delta S^0_C/2$:

$$v_{f=0} = \frac{d[e^{\Delta S^0_C/(2k_B)} - 1]}{e^{\Delta S^0_C/(2k_B)}(k_{12}^{-1} + k_{34}^{-1}) + k_{21}^{-1} + k_{43}^{-1}}. \tag{14}$$

Eq. (13) is used to derive the load dependence of the velocity by introducing the optimization condition $\Delta S_{23} = \Delta S_{41} = \Delta S^0_{23} - fd/(2T)$ as well as the load dependence of the transition rates. The derived expression is

$$v = \frac{de^{\Delta S^0_{23}/k_B}e^{-fd/(2k_BT)} - 1}{e^{-fd/(2k_BT)}e^{f(\delta_0+\varepsilon f)/(k_BT)}\{e^{\Delta S^0_{23}/k_B}[(k^0_{23})^{-1} + (k^0_{41})^{-1}] + (k^0_{32})^{-1} + (k^0_{14})^{-1}\}}. \tag{15}$$

Applying the approximation $e^{\Delta S23/k_B} \gg 1$ and replacing the zero-load velocity with Eq. (14) yields Eq. (7).

5.3 Expression for the stepping ratio

The stepping ratio, $R = (p_2k_{23} + p_4k_{41})/(p_3k_{32} + p_1k_{14})$, can be simplified by introducing the condition $\Delta S_{23} = \Delta S_{41}$, which yields $R = e^{\Delta S23/k_B} = e^{\Delta S41/k_B}$. Replacing ΔS_{23} in the expression with its form in Eq. (5) gives $R = e^{[\Delta\mu\prime - T(\Delta S12 + \Delta S34)]/(2k_BT)}\cdot e^{-f(d/2)/(k_BT)}$. The assumption of small $\Delta S_{12} + \Delta S_{34}$ suggests that the sum can be replaced by ΔS^0_C without affecting the value of R, yielding Eq. (8).

5.4 Expression for the dwell time

The relationship between the velocity (v) and average dwell time (τ) over all steps is $v = [(p_2k_{23} - p_3k_{32} + p_4k_{41} - p_1k_{14})d/2]/[(p_2k_{23} + p_3k_{32} + p_4k_{41} + p_1k_{14})\tau/2]$. Replacing the velocity with Eq. (7) and the transition fluxes with the stepping ratio [$R = (p_2k_{23} + p_4k_{41})/(p_3k_{32} + p_1k_{14})$] gives the expression for the dwell time in Eq. (9).

5.5 Elongation coefficient ε

In state 2 (Fig. 1), the load force (f) pulls the neck linker with the track-bound head toward the minus end of the track. The wormlike chain model with a Gaussian approximation gives the force–extension relation of the neck linker: $f = [k_BT/(l_pl_c)]l$, where l is the extension. In state 3, because both heads are bound to the track, the load force extends the neck linker on the plus-end side but reduces it on the minus-end side, and the force–extension relation is $f = [k_BT/(l_pl_c)](l_1 - l_2)$, where l_1 and l_2 are the extensions for the two neck linkers. Hence, the load-coupling distance is elongated by the distance $l - (l_1 - l_2)/2 = [l_pl_c/(2k_BT)]f$, and the coefficient ε equals $l_pl_c/(2k_BT)$.

Acknowledgements This work was supported by the National Natural Science Foundation of China under Grant No. 11774284 (to H. R. Li) and Grant No. 11534008.

References

1. R. D. Vale and R. A. Milligan, The way things move: Looking under the hood of molecular motor proteins,

Science 288(5463), 88 (2000)

2. R. D. Vale, The molecular motor toolbox for intracellular transport, *Cell* 112(4), 467 (2003)
3. S. Rice, A. W. Lin, D. Safer, C. L. Hart, N. Naber, B. O. Carragher, S. M. Cain, E. Pechatnikova, E. M. Wilson-Kubalek, M. Whittaker, E. Pate, R. Cooke, E. W. Taylor, R. A. Milligan, and R. D. Vale, A structural change in the kinesin motor protein that drives motility, *Nature* 402(6763), 778 (1999)
4. S. Rice, Y. Cui, C. Sindelar, N. Naber, M. Matuska, R. Vale, and R. Cooke, Thermodynamics properties of the kinesin neck-region docking to the catalytic core, *Biophys. J.* 84(3), 1844 (2003)
5. K. Visscher, M. J. Schnitzer, and S. M. Block, Single kinesin molecules studied with a molecular force clamp, *Nature* 400(6740), 184 (1999)
6. N. J. Carter and R. A. Cross, Mechanics of the kinesin step, *Nature* 435(7040), 308 (2005)
7. M. Nishiyama, H. Higuchi, and T. Yanagida, Chemomechanical coupling of the forward and backward steps of single kinesin molecules, *Nat. Cell Biol.* 4(10), 790 (2002)
8. Y. Taniguchi, M. Nishiyama, Y. Ishii, and T. Yanagida, Entropy rectifies the Brownian steps of kinesin, *Nat. Chem. Biol.* 1(6), 342 (2005)
9. M. J. Schnitzer, K. Visscher, and S. M. Block, Force production by single kinesin motors, *Nat. Cell Biol.* 2(10), 718 (2000)
10. S. Liepelt and R. Lipowsky, Kinesin's network of chemomechanical motor cycles, *Phys. Rev. Lett.* 98(25), 258102 (2007)
11. S. Liepelt and R. Lipowsky, Steady-state balance conditions for molecular motor cycles and stochastic nonequilibrium processes, *EPL* 77(5), 50002 (2007)
12. Z. S. Wang, M. Feng, W. W. Zheng, and D. G. Fan, Kinesin is an evolutionarily fine-tuned molecular ratchet-and-pawl device of decisively locked directionality, *Biophys. J.* 93(10), 3363 (2007)
13. D. G. Fan, W. W. Zheng, R. Hou, F. Li, and Z. S. Wang, Modelling motility of the kinesin dimer from molecular properties of individual monomers, *Biochemistry* 47(16), 4733 (2008)
14. R. D. Astumian, Thermodynamics and kinetics of molecular motors, *Biophys. J.* 98(11), 2401 (2010)
15. R. D. Astumian, Irrelevance of the power stroke for the directionality, stopping force, and optimal efficiency of chemically driven molecular machines, *Biophys. J.* 108(2), 291 (2015)
16. J. Ren, Detectable states, cycle fluxes, and motility scaling of molecular motor kinesin: An integrative kinetic graph theory analysis, *Front. Phys.* 12(6), 120505 (2017)
17. B. E. Clancy, W. M. Behnke-Parks, J. O. L. Andreasson, S. S. Rosenfeld, and S. M. Block, A universal pathway for kinesin stepping, *Nat. Struct. Mol. Biol.* 18(9), 1020 (2011)
18. R. A. Cross, The kinetic mechanism of kinesin, *Trends Biochem. Sci.* 29(6), 301 (2004)
19. B. Milic, J. O. L. Andreasson, W. O. Hancock, and S. M. Block, Kinesin processivity is gated by phosphate release, *Proc. Natl. Acad. Sci. USA* 111(39), 14136 (2014)
20. K. J. Mickolajczyk, N. C. Deffenbaugh, J. Ortega Arroyo, J. Andrecka, P. Kukura, and W. O. Hancock, Kinetics of nucleotide-dependent structural transitions in the kinesin-1 hydrolysis cycle, *Proc. Natl. Acad. Sci. USA* 112(52), E7186 (2015)
21. G. Y. Chen, D. F. J. Arginteanu, and W. O. Hancock, Processivity of the kinesin-2 KIF3A results from rear head gating and not front head gating, *J. Biol. Chem.* 290(16), 10274 (2015)
22. A. Efremov and Z. S. Wang, Universal optimal working cycles of molecular motors, *Phys. Chem. Chem. Phys.* 13(13), 6223 (2011)
23. U. Seifert, Entropy production along a stochastic trajectory and an integral fluctuation theorem, *Phys. Rev. Lett.* 95(4), 040602 (2005)
24. J. Schnakenberg, Network theory of microscopic and macroscopic behavior of master equation systems, *Rev. Mod. Phys.* 48(4), 571 (1976)
25. M. Rubinstein and R. H. Colby, Polymer Physics, Oxford: Oxford University Press, 2003
26. I. Schwaiger, C. Sattler, D. R. Hostetter, and M. Rief, The myosin coiled-coil is a truly elastic protein structure, *Nat. Mater.* 1(4), 232 (2002)
27. R. Yasuda, H. Noji, K. Jr Kinosita, and M. Yoshida, F_1–ATPase is a highly efficient molecular motor that rotates with discrete 120° steps, *Cell* 93(7), 1117 (1998)
28. S. Toyabe, T. Watanabe-Nakayama, T. Okamoto, S. Kudo, and E. Muneyuki, Thermodynamic efficiency and mechanochemical coupling of F-1-ATPase, *Proc. Natl. Acad. Sci. USA* 108(44), 17951 (2011)
29. S. Toyabe and E. Muneyuki, Single molecule thermodynamics of ATP synthesis by F-1-ATPase, *New J. Phys.* 17(1), 015008 (2015)
30. R. Z. Hou and Z. S. Wang, Role of directional fidelity in multiple aspects of extreme performance of the F-1-ATPase motor, *Phys. Rev. E* 88(2), 022703 (2013)
31. Z. S. Wang, R. Z. Hou, and A. Efremov, Directional fidelity of nanoscale motors and particles is limited by the 2nd law of thermodynamics-Via a universal equality, *J. Chem. Phys.* 139(3), 035105 (2013)
32. Z. S. Wang, Synergic mechanism and fabrication target for bipedal nanomotors, *Proc. Natl. Acad. Sci. USA* 104(46), 17921 (2007)
33. J. Cheng, S. Sreelatha, R. Z. Hou, A. Efremov, R. C. Liu, J. R. C. van der Maarel, and Z. S. Wang, Bipedal nanowalker by pure physical mechanisms, *Phys. Rev. Lett.* 109(23), 238104 (2012)
34. M. H. Liu, R. Z. Hou, J. Cheng, L. Y. Loh, S. Sreelatha, J. N. Tey, J. Wei, and Z. S. Wang, Autonomous synergic control of nanomotors, *ACS Nano* 8(2), 1792 (2014)

35. I. Y. Loh, J. Cheng, S. R. Tee, A. Efremov, and Z. Wang, From bistate molecular switches to self-directed track-walking nanomotors, *ACS Nano* 8(10), 10293 (2014)

36. R. Hou, I. Y. Loh, H. Li, and Z. Wang, Mechanical-kinetic modeling of a molecular walker from a modular design principle, *Phys. Rev. Appl.* 7(2), 024020 (2017)

37. R. D. Astumian, Thermodynamics and kinetics of a Brownian motor, *Science* 276(5314), 917 (1997)

38. S. Uemura, H. Higuchi, A. O. Olivares, E. M. De La Cruz, and S. Ishiwata, Mechanochemical coupling of two substeps in a single myosin V motor, *Nat. Struct. Mol. Biol.* 11(9), 877 (2004)

39. N. Soga, K. Kimura, M. Jr Kinosita, Yoshida, and T. Suzuki, Perfect chemomechanical coupling of FoF1-ATP synthase, *Proc. Natl. Acad. Sci. USA* 114(19), 4960 (2017)